arXiv:1603.05288v2 [cond-mat.supr-con] 17 May 2016

Tracing the electronic pairing glue in unconventional superconductors via Inelastic Scanning Tunneling Spectroscopy

Patrik Hlobil,[1,2,3] Jasmin Jandke,[4] Wulf Wulfhekel,[4] and Jörg Schmalian[2,3]

[1] *Corresponding author*

[2] *Institut für Festkörperphysik, Karlsruher Institut für Technologie, 76344 Karlsruhe, Germany*

[3] *Institut für Theorie der Kondensierten Materie, Karlsruher Institut für Technologie, 76131 Karlsruhe, Germany*

[4] *Physikalisches Institut, Karlsruher Institut für Technologie, 76131 Karlsruhe, Germany*

(Dated: May 18, 2016)

PACS numbers: 74.55.+v, 74.20.Mn, 74.20.Rp, 74.70.Xa

The origin of Cooper pairing in high-temperature superconductors, such as cuprates and iron-based superconductors, is still under debate. Scanning tunneling microscopy (STM) has been shown to be a powerful experimental probe to detect electronic excitations and further allows to deduce fingerprints of bosonic collective modes. Here, we demonstrate that the inclusion of inelastic tunnel events is crucial for the interpretation of tunneling spectra of unconventional superconductors and allows to directly probe electronic and bosonic excitations via STM. Adopting this extended tunneling formalism we can naturally reproduce the tunneling spectra of various unconventional superconductors and trace the occurring features back to an opening of a gap in the spectrum of the pairing glue below T_c. Thus, with the inclusion of inelastic contributions, a non-conventional pairing mechanism, likely via magnetic excitations can be experimentally verified. Specifically, our approach gives evidence for a collective mode mediating an unconventional sign-changing pairing state for LiFeAs.

Electron tunneling spectroscopy has turned out to be an outstanding tool for the investigation of superconductors. For example, exploiting the local resolution of STM, quasiparticles interference spectroscopy exploits standing waves due to impurity scattering in a correlated material[1–3] to obtain momentum space information. A classical result of tunneling spectroscopy is of course the determination of the superconducting *pairing glue* in many materials, especially in the case of conventional phonon-pairing[4,5]. Conventional elastic tunneling theory[6,7] interprets the conductance to be proportional to the electronic density of states (DOS) for low temperatures. In Bardeen-Cooper-Schrieffer (BCS) theory, the coupling to phonons was approximated to be energy and momentum independent in an energy range around the Fermi energy set by the Debye frequency leading to the well known coherence peaks outside/at the superconducting gap Δ (see Figure 1a, black curve). In strong coupling theory[8], both an energy dependent coupling to phonons and the details of the phonon DOS enter, leading to renormalization of the electronic DOS above the coherence peaks and causing peak-dip features on top of the BCS-DOS, as seen by elastic tunneling[4]. In cuprate and iron-based superconductors, similar peak-dip features in the conductance of tunneling experiments have been intensely investigated[9–24]. The most frequent interpretation is based

on elastic tunneling theory in terms of a renormalization of the electronic spectral function by coupling of electrons to a sharp spin resonance mode with frequency $\omega_{\rm res}$ and with momentum at the antiferromagnetic ordering vector of the material [25–27]. This resonance mode is of course well established by inelastic neutron scattering[28–31] and has left traces in other experimental techniques as well[32–34].

With STM an electron-boson coupling can also lead to the inelastic emission of real bosons in a scattering event during the tunneling process. An inelastic tunneling event is depicted in Fig. 1b: A tip-electron tunnels elastically into a high-energy off-shell state far away from the Fermi surface of the superconductor from where the electron scatters inelastically via the emission/absorption of a boson to a state near the Fermi-surface. Inelastic tunneling has been observed for conventional superconductors in the normal state[35,36] and has recently been shown to be of importance even in the superconducting state of Pb-films[37]. Furthermore, in the normal state of the cuprate superconductors it is well established that inelastic tunneling channels are present and in general not negligible[10,20,38–42]. They give rise to the frequently observed V-shape of the normal state spectrum closely tied to an overdamped particle-hole spectrum as depicted by the blue curve in Figure 1a. Such V-shaped background conductances have also been seen in the iron pnictide superconductors[13,23,24]. Also, the inclusion of inelastic tunneling in the superconducting state of unconventional superconductors is not only necessary, it does, as we will show, allow for a direct investigation of electronic and bosonic excitations via STM. Whether the conventional interpretation of the STM fine-structures requires revision is then an important open question.

The ability to simultaneously probe the electronic and bosonic excitation spectrum is particularly appealing as it allows to distinguish between conventional and electronic driven pairing mechanisms. In the latter one expects a dramatic reorganization of the glue-boson spectrum in the superconducting state. Due to the opening of the superconducting gap below the transition temperature T_c, the spin or charge excitation spectrum is gapped at low energies. In case of the spin-spectrum, the gap is the resonance mode energy $\omega_{\rm res}$ in the case of unconventional pairing.

We here propose to describe both elastic and inelastic tunneling into unconventional superconductors driven by spin fluctuations. The approach reproduces the resonance mode leading to moderate Eliashberg features at the superconducting gap Δ plus the resonance mode $\omega_{\rm res}$ in the elastic channel (green curve in Fig. 1a) but introduces strong inelastic

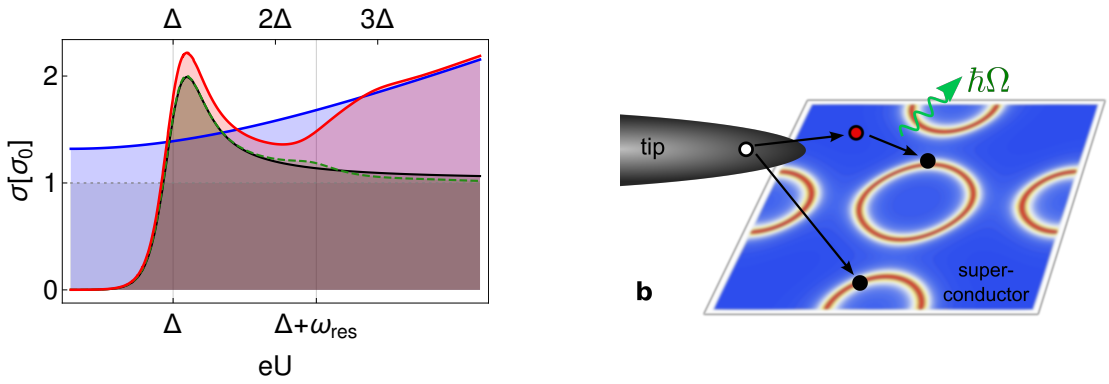

FIG. 1: **STM spectra expected for a system with resonance mode and sketch of elastic and inelastic tunneling processes. a**, The differential conductance $\sigma(U) = dI/dU$ is calculated from the sum of elastic and inelastic tunneling currents $I = I^{\mathrm{e}} + I^{\mathrm{i}}$ normalized to the purely elastic conductance σ_0 in the normal state. Shown are in black the elastic spectrum of the simple BCS state, in green the strong-coupling elastic spectrum for electrons coupled to a spin mode, in blue the total elastic and inelastic spectrum in the normal state and in red the total spectrum in the superconducting state with superconducting gap Δ and resonance mode ω_{res} (red), as function of applied bias U. For a gapped bosonic spectrum a clear peak-dip-hump feature is visible as well as a V-shaped conductance background in the normal state. The temperature has been set to 0.1 Δ for the superconducting spectra and 0.5 Δ for the normal spectra. **b**, The inelastic tunneling process involves a intermediate off-shell state far away from the Fermi surface, which is then scattered inelastically via the emission/absorption of a boson to a state near the superconducting Fermi surface.

contributions due to coupling to all bosonic modes (red curve in Fig. 1a). The latter are gapped by $\Delta + \omega_{\mathrm{res}}$ in the superconducting state. If compared with the V-shaped normal state background conductance, the total conductance in the superconducting state is suppressed for energies above the coherence peak and below $\Delta+\omega_{\mathrm{res}}$ in agreement with many experimentally observed tunneling spectra of diverse unconventional superconductors, e.g. in YBCO[14] and LiFeAs[13]. Thus, the dominance of inelastic contributions to the tunneling spectra for various unconventional superconductors pinpoints the relevance of an electronic glue of Cooper pairing.

The distinction between elastic and inelastic tunneling is ultimately based on the view that the electronic spectrum is subdivided into a low-energy renormalized quasiparticle regime and high-energy off-shell states. Usually, many-body interactions are analysed for

the renormalized quasiparticle excitations, e.g. in the celebrated Eliashberg formalism[8]. However, tunneling processes into off-shell states far away from the Fermi surface may subsequently relax into states near the Fermi energy via the emission of a bosonic excitation. This is a process with a large phase space as long as the typical bosonic momentum is large, examples are zone-boundary phonons or antiferromagnetic fluctations.

In the following, we develop a theory describing the tunneling spectra between a superconductor and a normal metal from a microscopic model including *elastic* and *inelastic* tunneling channels. The corresponding low energy Hamiltonian is of the following form:

$$\mathcal{H}_{\text{tun}}^{\text{eff}} = \sum_{\substack{\boldsymbol{k},\boldsymbol{k}'\\ \sigma,\sigma'}} \left[t^{\text{e}}_{\boldsymbol{k},\boldsymbol{k}'} \delta_{\sigma,\sigma'} + \sum_{\boldsymbol{q}} t^{\text{i},\sigma,\sigma',n}_{\boldsymbol{k},\boldsymbol{k}',\boldsymbol{q}} \cdot \hat{\Phi}^n_{\boldsymbol{q}} \right] \hat{c}^\dagger_{\boldsymbol{k},\sigma,s} \hat{c}_{\boldsymbol{k}',\sigma',t} \,, \tag{1}$$

where $t^{\text{e}}_{\boldsymbol{k},\boldsymbol{k}'}$ and $t^{\text{i},\sigma,\sigma',n}_{\boldsymbol{k},\boldsymbol{k}',\boldsymbol{q}}$ are the elastic and inelastic tunneling matrix elements for electrons tunneling between the superconductor and the normal tip of an scanning tunneling microscope. $\boldsymbol{k}$ and σ are the wave vector and spin degrees of freedom. For simplicity, we omit band indices. The operators $\hat{\Phi}^n_{\boldsymbol{q}}$ with mode index $n = 1, \ldots, \mathcal{N}$ depicts the relevant collective bosonic degrees of freedom in the superconductor, whose dynamics are governed by the bare boson Hamiltonian $\mathcal{H}_{\Phi,0}$. Finally we define the creation operator $\hat{c}^\dagger$ for the electrons in the superconductor s and the tip t.

We obtain this low energy Hamiltonian from the generic, *purely elastic* high-energy tunnel Hamiltonian including a Yukawa-like electron-boson coupling

$$\mathcal{H}_0 = \sum_{\boldsymbol{k},\sigma=\uparrow,\downarrow} \left[\epsilon^s_{\boldsymbol{k}} \hat{c}^\dagger_{\boldsymbol{k},\sigma,s} \hat{c}_{\boldsymbol{k},\sigma,s} + \epsilon^t_{\boldsymbol{k}} \hat{c}^\dagger_{\boldsymbol{k},\sigma,t} \hat{c}_{\boldsymbol{k},\sigma,t} \right] + \sum_{\substack{\boldsymbol{k},\boldsymbol{q}\\ \sigma,\sigma',n}} \hat{c}^\dagger_{\boldsymbol{k}+\boldsymbol{q},\sigma,s} \alpha^n_{\boldsymbol{q},\sigma,\sigma'} \hat{c}_{\boldsymbol{k},\sigma',s} \hat{\Phi}^n_{\boldsymbol{q}} + \mathcal{H}_{\Phi,0} + \mathcal{H}_{\text{el-el}} \,, \tag{2}$$

$$\mathcal{H}^0_{\text{tun}} = \sum_{\substack{\boldsymbol{k},\boldsymbol{k}'\\ \sigma}} \left[t^{\text{e}}_{\boldsymbol{k},\boldsymbol{k}'} \hat{c}^\dagger_{\boldsymbol{k},\sigma,s} \hat{c}_{\boldsymbol{k}',\sigma,t} + \text{h.c.} \right] . \tag{3}$$

Here, $\epsilon^{s/t}_{\boldsymbol{k}}$ is the dispersions of the electrons in the superconductor/tip, the coupling of the bosonic modes to the electrons is described via the interaction vertex $\alpha^n_{\boldsymbol{q},\sigma,\sigma'}$ and the screened electron-electron interaction is given by $\mathcal{H}_{\text{el-el}}$. Importantly, the momentum sums for the electronic degrees of freedom cover the entire Brillouin zone, such that we can introduce a high-energy cutoff $E_{\text{c}} \sim D$ of the scale of the band-width D of the superconductor (and tip). From this *elastic* high-energy tunneling Hamiltonian $\mathcal{H} = \mathcal{H}_0 + \mathcal{H}^0_{\text{tun}}$ one obtains the effective low-energy theory (1) by integrating out the off-shell electrons with energy

$\omega > E_{\rm ME}$, where $E_{\rm ME}$ is the energy scale of the Migdal-Eliashberg theory which is typically of the order of the maximum bosonic energy[43]. Approximating the dynamic propagator of the off-shell electrons, see Supplementary Material, one obtains the low-energy Hamiltonian $\mathcal{H}_{\rm eff} = \mathcal{H}_0^{\rm ME} + \mathcal{H}_{\rm tun}^{\rm eff}$ that includes an inelastic tunneling term of the form (1). Here, $\mathcal{H}_0^{\rm ME}$ is the Hamiltonian in (2) with the renormalized electron-boson and electron-electron interaction of the superconducting Migdal-Eliashberg low-energy theory[43] restricted to electronic states with energies $\omega < E_{\rm ME}$. Within this theory the inelastic tunneling matrix elements reads

$$t^{{\rm i},\sigma,\sigma',n}_{\boldsymbol{k},\boldsymbol{k}',\boldsymbol{q}} = \frac{\alpha^n_{\boldsymbol{q},\sigma,\sigma'} t^{\rm e}_{\boldsymbol{k}-\boldsymbol{q},\boldsymbol{k}'}}{D}\,. \tag{4}$$

Our formalism can easily be extended to inelastic tunneling channels involving the multiple emission/absorption of N bosons, where the matrix element scales with $t^{\rm e}(\alpha/D)^N$, such that in general such contributions will be suppressed as the band width D is usually the largest energy scale of the system.

In the following, we investigate how inelastic tunneling affects the tunneling spectra in unconventional superconductors. We consider the special case of a spin-fermion coupling proposed as an effective model for various unconventional superconductors[42]. Here, the relevant collective bosonic degrees of freedom can be written in terms of a 3-component spin vector $\Phi^n_{\boldsymbol{q}} \to \boldsymbol{S}_{\boldsymbol{q}} = (S^1_{\boldsymbol{q}}, S^2_{\boldsymbol{q}}, S^3_{\boldsymbol{q}})^T$ with a Yukawa-like electron-boson coupling

$$\sum_{\substack{\boldsymbol{k},\boldsymbol{k}'\\ \sigma,\sigma'}} g_{\boldsymbol{k}-\boldsymbol{k}'} \big(\hat{c}^\dagger_{\boldsymbol{k},\sigma,s} \boldsymbol{\tau}_{\sigma,\sigma'} \hat{c}_{\boldsymbol{k}',\sigma',s}\big) \cdot \boldsymbol{S}_{\boldsymbol{k}-\boldsymbol{k}'}, \tag{5}$$

with the Pauli-matrices τ^i. Thus, the inelastic tunneling matrix element reads $t^{\rm i}_{\boldsymbol{k},\boldsymbol{k}',\sigma,\sigma'} = \sum_{\boldsymbol{q}} \big(g_q t^{\rm e}_{\boldsymbol{k}+\boldsymbol{q},\boldsymbol{k}'}/D\big)\, \boldsymbol{\tau}_{\sigma,\sigma'} \cdot \boldsymbol{S}_{\boldsymbol{q}}$. The predicted current is the sum $I = I^{\rm e} + I^{\rm i}$ of the elastic and inelastic contributions. Following Jandke *et al.*[37] we find for $t^{\rm e}_{\boldsymbol{k},\boldsymbol{p}} \approx t^{\rm e}$[44] and a constant tip DOS the two contributions to the differential conductance $\sigma(U) = dI/dU$[38,39]

$$\sigma^{\rm e}(U) = -\sigma_0 \int_{-\infty}^{\infty} d\omega\, n'_F(\omega + eU)\, \tilde{\nu}_S(\omega)\,, \tag{6}$$

$$\begin{aligned}\sigma^{\rm i}(U) = -\frac{\sigma_0}{D^2 \nu_S^0} \int_{-\infty}^{\infty} d\omega_1 d\omega_2\, g^2 \chi(\omega_1)\, \tilde{\nu}_S(\omega_2) \\ \Big[n'_F(\omega_2 - \omega_1 + eU) n_B(\omega_1) \big[1 - n_F(\omega_2)\big] + n_F(\omega_2) \big[1 + n_B(\omega_1)\big] n'_F(\omega_2 - \omega_1 + eU) \\ + n'_F(\omega_2 + \omega_1 + eU) \big[1 + n_B(\omega_1)\big] \big[1 - n_F(\omega_2)\big] + n_F(\omega_2) n_B(\omega_1) n'_F(\omega_2 + \omega_1 + eU) \Big]\,,\end{aligned} \tag{7}$$

where U is the applied voltage, $\sigma_0 = 4\pi e^2 \left|t^{\rm e}\right|^2 \nu_T^0 \nu_S^0$ and $\nu^0_{S/T}$ are the normal state DOS of the superconductor and the tip at the Fermi energy. We also define the normalized

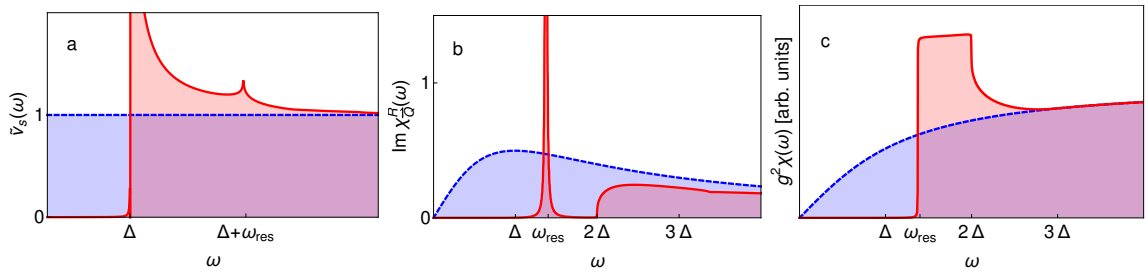

FIG. 2: **Calculated spectra for the spin electron model in the normal (blue) and superconducting state (red): a**, Electronic density of states. **b**, Spin spectrum $\mathrm{Im}\,\chi^R_{\boldsymbol{Q}}(\omega)$ at the antiferromagnetic ordering vector $\boldsymbol{Q}$ with the resonance mode occurring at ω_{res} below T_c. **c**, spin spectrum $g^2\chi$ integrated over the 2-dimensional Brillouin zone.

electronic DOS $\tilde{\nu}_S(\omega) = \nu_S(\omega)/\nu_S^0$ and the dimensionless, integrated bosonic spin spectrum in the superconductor $g^2\chi(\omega) = -3\nu_S^0 \int d^2\boldsymbol{q}\, |g_{\boldsymbol{q}}|^2\, \mathrm{Im}\,\chi^R_{\boldsymbol{q}}(\omega)/\pi$.

In order to calculate the two contributions to the tunneling current, we need information about the electronic and bosonic spectra. Here, we follow Abanov *et al.*[45] for their calculation in the normal and superconducting state. Above T_c the spin susceptibility shows an overdamped behaviour according to $\left[\chi^R_{\boldsymbol{q}}(\omega)\right]^{-1} \sim 1 + \xi^2(\boldsymbol{q}-\boldsymbol{Q})^2 - \Pi^R_{\boldsymbol{Q}}(\omega)/\omega_{\mathrm{sf}}$ with $\Pi^R_{\boldsymbol{Q}}(\omega) = i\omega$ (see blue curve in Fig. 2b). Here, $\boldsymbol{Q}$ is the antiferromagnetic ordering vector and ω_{sf} the characteristic energy scale of the boson. The latter is inversely proportional to the square of the magnetic correlation length ξ and typically of the order of the superconducting gap Δ[31,46,47]. Below T_c one can solve the Eliashberg equations numerically[48], which we do for a nodeless pairing state here. As usual, the sign of the gap changes between states that are connected by the magnetic wave vector. In the following we have chosen our input parameters ω_{sf}, λ of the theory in such a way that the observed gap and spin spectrum agrees well with the experimental observations[30,31,46,47] $\omega_{sf} \simeq \Delta$ and $\omega_{\mathrm{res}}/2\Delta \approx 0.7$. However, we note that the main conclusions of our calculations are not affected by changing these numbers within reasonable ranges.

In the superconducting state $T < T_c$ a spin gap evolves as the energy of 2Δ is needed to break up a Cooper pair and to create a particle-hole excitation. Thus, spin spectral weight is shifted to higher energies by the opening of the superconducting gap Δ for the electronic quasiparticles. This is in contrast to conventional superconductors, where the phonon modes are only weakly renormalized below T_c. Thus, in unconventional superconductors, it is essen-

tial to solve the coupled Eliashberg equations for the electrons and bosons self-consistently. For a sign-changing gap symmetry $\Delta := \Delta_{\boldsymbol{k}_h} = -\Delta_{\boldsymbol{k}_h+\boldsymbol{Q}}$ (e.g. d-wave or $s_\pm$-wave depending on the details of the electronic structure) a sharp resonance peak occurs near the antiferromagnetic wave vector $\boldsymbol{Q}$ and the energy $\omega_{\rm res} < 2\Delta$[42,45] (see red curve in Fig. 2b), which leads to a spin gap of $\omega_{\rm res}$ in the integrated spectrum $g^2\chi(\omega)$ (see red curve in Fig. 2c). For the electronic degrees of freedom a superconducting gap Δ appears and due to the coupling to the spin resonance mode a strong coupling feature in the electronic DOS $\tilde{\nu}_s(\omega)$ evolves at $\Delta + \omega_{\rm res}$ (see red curve of Fig. 2a). Note, that there is no pronounced dip as the spectral weight of the sharp resonance mode is small compared to the total integrated spin spectrum. In case of nodal superconductivity, our theory is not capable of reproducing the density of states in the gap region and we concentrate our analysis to fully gapped systems or features above the quasiparticle peak where possible nodal excitations are unimportant.

The calculated electronic DOS and integrated spin spectrum $g^2\chi(\omega)$ shown in Fig. 2 are finally used to calculate the elastic and inelastic contributions to the conductance via Eqs. (6, 7). We choose $T = 0.1\Delta$ for the superconducting and $T = 0.5\Delta$ for the normal state calculations. The elastic conductance reflects the DOS of the superconductor including thermal smearing, which is constant for the normal state in our model (see blue curve in Fig. 3a). For $T < T_c$ we see the quasiparticle peak at $\omega = \Delta$ as well as the thermally broadened strong-coupling peak-dip features at $\Delta + \omega_{\rm res}$ due to coupling to the resonance mode. In contrast to the elastic conductance in the normal state, the *inelastic* conductance shows a typical V-shape structure similar to the spectra calculated in earlier theoretical publications[40,41] as inelastic processes open up additional tunneling channels for both positive and negative bias U (see blue curve in Fig. 3b). Besides the V-shape, there are no clear features visible for $T > T_c$ since the overdamped mode only shows little structure in energy, especially after the integration over the Brillouin zone. We note that for a fixed tunnel parameter $t^{\rm e}$ the inelastic contribution to the current is temperature dependent. Therefore, the differential conductance spectra for the same tunnel parameters for different temperatures do not need to lie on top of each other even for high biases if inelastic tunneling is present. Note that the inelastic contributions vanish at zero bias only for $T = 0$.

In the superconducting state $T < T_c$ the following features arise in the tunneling spectrum: The *elastic* tunneling contribution seen in Fig. 3a (red curve) is proportional to the the thermally smeared electronic DOS with the gap Δ, the coherence peak at Δ followed by the

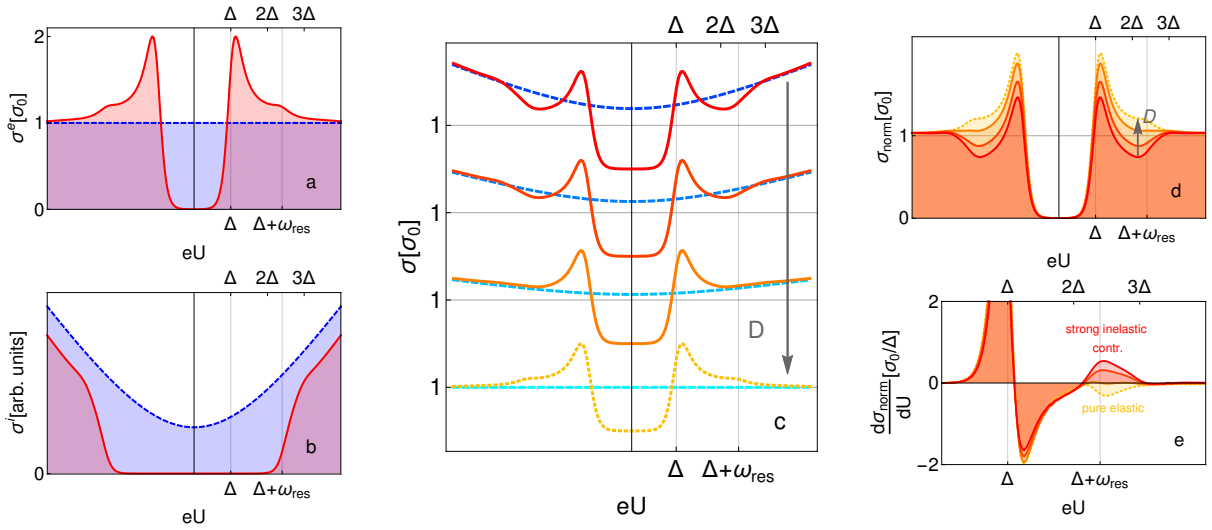

FIG. 3: **Calculated conductance for the spin-fermion model:** Shown are the elastic (**a**) and inelastic (**b**) contributions to the conductance both in the superconducting (red, orange) and normal state (blue) tunneling spectra for different inelastic tunneling amplitudes (energy cutoffs D (**c**) (increasing D lowers inelastic contributions), normalized conductance $\sigma_{\rm norm}(U) = \sigma_{\rm sc}(U)/\sigma_{\rm nc}(\sqrt{U^2-(\Delta/e)^2})$ (**d**) and derivative of the normalized conductance (**e**). The tunneling parameters are set such that the current I at $eU = 10\Delta$ is the same for the normal and superconducting state.

usual peak-dip strong-coupling features seen at $\Delta+\omega_{\rm res}$ that quickly approaches the assumed constant DOS of the normal state for higher biases. In contrast, the *inelastic* tunneling conductance seen in Fig. 3b (red curve) is gapped by $\Delta + \omega_{\rm res}$ as both the electronic DOS and the bosonic spectrum obtain a gap below T_c. For voltages $eU > \Delta + \omega_{\rm res}$ the inelastic differential conductance shows a sharp increase but does stay below the normal state inelastic conductance due to the different temperatures as explained above. The shape can be traced back to the fact that spin spectral weight is shifted from lower to higher energies, mostly close above the resonance mode at the frequency $\omega_{\rm res}$.

Naturally, only the sum of the two contributions $\sigma = \sigma^{\rm e} + \sigma^{\rm i}$ is observable in experiments posing a normalization issue for STM measurements. In these, the total conductance is set by the bias voltage and current of the feedback loop. Here, we set the tunneling parameters such that the current I at $U = 10\Delta$ is the same for the normal and superconducting state. Fig. 3c depicts the resulting total conductance including the normalization for different energy cutoffs D. For weak inelastic contributions (g/D small) mainly the quasiparticle peak

at Δ is visible on top of a small inelastic increase at high energies. The Eliashberg-features of the resonance mode are already obscured by the inelastic contributions (yellow curve). If we increase the inelastic tunneling amplitude we see that the conductance in the superconducting state is lowered in contrast to the normal state at $eU \approx 2\Delta$ due to the loss of spin spectral weight as was stated above. Due to the normalization procedure, the superconducting conductance is slightly larger for energies above $\gtrsim 3\Delta$. We note, that the obtained spectra look similar to the many measured differential conductances[10,13–22], especially the fact that the superconducting differential conductance dips below the normal differential conductance above the quasiparticle peak followed by a V-shaped background conductance at higher energies. For d-wave superconductors it was also shown that a pronounced peak can occur at $\Delta + \omega_{\mathrm{res}}$ due to the coupling to a sharp bosonic mode[9], which will then even enhance the dip seen in the spectra that show such a background conductance. Note, that in many high-temperature superconductors the electronic spectrum in the normal state is non-flat. Thus, already the electronic DOS and therefore also the elastic conductance shows a clear energy-dependence around the Fermi edge. One way to treat this is to include variations of the DOS in (6,7), which does not alter the main conclusions, or to normalize the experimental spectra with the normal state conductance.

In Fig. 3a we plot the normalized conductance $\sigma_{\mathrm{norm}}(U) = {}^{\sigma_{\mathrm{sc}}(U)}/_{\sigma_{\mathrm{nc}}(\sqrt{U^2-(\Delta/e)^2})}$, which facilitates a direct comparison with experiments as the effects of the a non-flat normal state DOS is reduced noticeably. Also here a significant loss of tunneling spectral weight can be seen in the superconductor for voltages $eU < \Delta + \omega_{\mathrm{res}}$, especially at $eU \approx 2\Delta$, and a following strong increase of the normalized conductance due to inelastic contributions from the scattering off the resonance mode. In the normalized second derivative this gives rise to a peak at $eU \approx \Delta + \omega_{\mathrm{res}}$. The obtained normalized spectrum fits well with tunneling data for various iron pnictide superconductors[13,23,24] and cuprate superconductors[14,19,20,49], except for the conductance in the gap region $eU < \Delta$ due to possible double gaps or different gap symmetries. Note that both the inelastic contributions and the Eliashberg-features of the resonance mode create signatures at similar energies, but the inelastic contributions create a peak in the second derivative (red curve in Fig. 3e for strong inelastic tunneling), while the Eliashberg-features create a dip at $\Delta + \omega_{\mathrm{res}}$ (yellow dotted curve in Fig. 3e for zero inelastic tunneling). As for unconventional pairing symmetry, the spin gap coincides with the resonance mode energy. Thus, the interpretation of various earlier publications[10,13,24]

are correct regarding the extracted resonance energy.

In case that already the normal differential conductance displays a V-shaped spectrum indicating the significance of inelastic contributions, our model suggests that the features in the superconducting tunneling spectra are dominated by inelastic effects of the gapped spin spectrum and Eliashberg-features only play a minor role. The model can be applied to a variety of unconventional superconductors in order to pinpoint the significance of spin fluctuations for the superconducting pairing. A prominent example of a hotly debated superconductor is LiFeAs[13]. The V-shaped normal state spectrum of this system is evidence for inelastic tunneling events, while fine structures above the largest gap are fully consistent with the behavior seen in our theory (note that the peak in the second derivative appears at energies $\approx 2.3\Delta$ consistent with a neutron resonance mode below 2Δ). Thus, we conclude that the pairing state of this system must be sign-changing, corresponding to an unconventional mechanism for superconductivity. In the future, this model including inelastic contributions may allow to invert the problem and to obtain the spectrum of the pairing glue from experimental tunneling spectra. The success of the presented analysis further confirms the view that a distinction of low-energy renormalized quasiparticles and high-energy off-shell states is the right one for system like the cuprate or iron-based superconductors.

The authors are grateful to Christian Hess, Pranab Kumar Nag and Rafael M. Fernandes for discussions and acknowledge funding by the DFG under the grant SCHM 1031/7-1 and WU 349/12-1.

Supplemental Material to "Tracing the electronic pairing glue in unconventional superconductors via inelastic Scanning Tunneling Spectroscopy"

DERIVATION OF LOW-ENERGY TUNNEL HAMILTONIAN

We start with the corresponding action to the high-energy transfer Hamiltonian given in the main part of the paper

$$S = S_{\Phi,0} + \int_{k,p} \hat{\psi}^\dagger_k \big[\hat{G}^{-1}_{k,0}\delta_{k,k'} + \hat{\Lambda}_{k,k'}\big]\hat{\psi}_{k'} \tag{8}$$

with the bare propagator and interaction matrix

$$\begin{aligned} \hat{G}^{-1}_{k,0} &= \mathrm{diag}\big([G^s_{k,0}]^{-1}, [G^t_{k,0}]^{-1}\big) \\ \hat{\Lambda}_{k,k'} &= -\begin{pmatrix} \sum_n \alpha^n_{k,k'}\Phi^n_{k-k'} & t^{\mathrm{e}}_{k,k'} \\ \bar{t}^{\mathrm{e}}_{k,k'} & 0 \end{pmatrix}. \end{aligned} \tag{9}$$

Here, we do not consider the repulsive electron-electron interaction, which will be renormalized in the usual way[43] for the low-energy theory. To derive this effective theory one separates the fermionic fields into low-energy modes and high-energy modes with respect to the smaller momentum cutoff $k_<$ of the low-energy theory

$$\hat{\psi}_k = \begin{cases} \hat{\psi}^<_k & \text{, for } |\boldsymbol{k} - \boldsymbol{k}_F| < k_< \\ \hat{\psi}^>_k & \text{, for } |\boldsymbol{k} - \boldsymbol{k}_F| > k_< \end{cases}. \tag{10}$$

Note, that here we assume the momentum cutoff for the tip and superconductor to be the same. We could easily assume different momentum cutoffs, but as we will later see the high-energy states of the tip will have no influence on the low-energy theory. The action can conveniently be rewritten as

$$S = S_{\Phi,0} + \int_{k,k'} \begin{pmatrix} \hat{\psi}^<_k \\ \hat{\psi}^>_k \end{pmatrix}^\dagger \begin{pmatrix} [\hat{G}^{<<}_{k,k'}]^{-1} & \hat{\Lambda}_{k,k'} \\ \hat{\Lambda}_{k,k'} & [\hat{G}^{>>}_{k,k'}]^{-1} \end{pmatrix} \begin{pmatrix} \hat{\psi}^<_{k'} \\ \hat{\psi}^>_{k'} \end{pmatrix}. \tag{11}$$

The bare dynamics of the low-energy and high-energy sectors are given by the $\hat{G}^{<<}_{k,k'}, \hat{G}^{>>}_{k,k'}$ propagators

$$\begin{aligned} [\hat{G}^{<<}_{k,k'}]^{-1} &= [\hat{G}^<_{k,0}]^{-1}\delta_{k,k'} + \hat{\Lambda}_{k,k'}, \\ [\hat{G}^{>>}_{k,k'}]^{-1} &= [\hat{G}^>_{k,0}]^{-1}\delta_{k,k'} + \hat{\Lambda}_{k,k'}, \end{aligned} \tag{12}$$

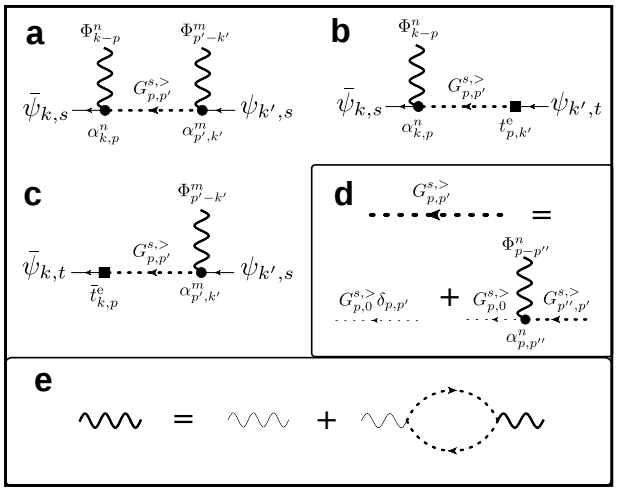

FIG. 4: **Interaction vertices generated by integrating out the high-energy fermions.** The diagram **a** gives describes scattering processes including an virtual off-shell state. The diagrams **b** and **c** describe the additional inelastic tunneling matrix element that emerge in the low-energy theory involving the high-energy propagator shown in **d**. The graph **e** describes the renormalization of the phonons in the superconductor due to the high-energy fermionic quasiparticles.

with the free high- and low-energy propagators

$$[\hat{G}^{>}_{k,0}]^{-1} = \hat{G}^{-1}_{k,0} \cdot \theta(|\boldsymbol{k} - \boldsymbol{k}_F| - k_<)\,,$$
$$[\hat{G}^{<}_{k,0}]^{-1} = \hat{G}^{-1}_{k,0} \cdot \theta(k_< - |\boldsymbol{k} - \boldsymbol{k}_F|)\,.$$

In contrast, the non-diagonal elements $\hat{\Lambda}_{k,k'}$ couple the $\hat{\psi}^{>}$ and $\hat{\psi}^{<}$ fields via the scattering with bosons and tunneling processes between the tip and the superconductor. Using the usual identities of Gaussian integrals we can integrate out the $\hat{\psi}^{>}$ field

$$\int D[(\hat{\psi}^{>})^{\dagger}, \hat{\psi}^{>}] e^{-S} = e^{-S_{\text{eff}}} \tag{13}$$

with the effective action

$$\begin{aligned} S_{\text{eff}} &= S_{\Phi,0} - \operatorname{tr}\ln[\hat{G}^{>>}] \\ &+ \int_{k,k'} \hat{\psi}^{<}_{k} \left([\hat{G}^{<<}_{k,k'}]^{-1} - \int_{p,p'} \hat{\Lambda}_{k,p} \hat{G}^{>>}_{p,p'} \Lambda_{p',k'} \right) \hat{\psi}^{<}_{k'}\,. \end{aligned} \tag{14}$$

The trace-log term will give rise to a bosonic self-energy (see polarization bubble in Fig. 4(e))

$$\operatorname{tr}\ln[\hat{G}^{>>}] = \frac{1}{2} \int_{\boldsymbol{q}} \Phi^{n}_{k-k'} \Phi^{m}_{-k+k'} \int_{k} \operatorname{tr}\left[\hat{G}^{>}_{k,0} \alpha^{n}_{k,k'} \hat{G}^{>}_{k',0} \alpha^{m}_{k',k} \right] + \mathcal{O}(\phi^4)\,, \tag{15}$$

which just describes the renormalization of the low-energy phonons due to the presence of the high-energy fermions. Importantly, the polarization operator is not depending on the elastic tunneling elements t^{e}, which only occur in the ϕ^4 terms and therefore the screening is in leading order not affected by the presence of the tunneling term in the Hamiltonian.
The other additional contribution for the low-energy theory is the last term in (14). For the evaluation we need to inverse of the second equation in (12), which has the formal solution

$$\hat{G}^{>,>}_{k,k'} = \hat{G}^{>}_{k,0}\delta_{k,k'} + \int_p \hat{G}^{>}_{k,0}\hat{\Lambda}_{k,p}\hat{G}^{>,>}_{p,k'} = \begin{pmatrix} \hat{G}^{>,>,ss}_{k,k'} & \hat{G}^{>,>,st}_{k,k'} \\ \hat{G}^{>,>,ts}_{k,k'} & \hat{G}^{>,>,tt}_{k,k'} \end{pmatrix} . \tag{16}$$

As can be easily seen from this expression, the propagators $\hat{G}^{>,>,st}_{k,k'}, \hat{G}^{>,>,ts}_{k,k'} \sim t^{\mathrm{e}}$ vanish for the uncoupled system. Using this property of $\hat{G}^{>,>}_{k,k'}$ it is straightforward to expand

$$\hat{\Lambda}_{k,p}\hat{G}^{>,>}_{p,p'}\Lambda_{p',k'} = G^{>,>,ss}_{p,p'}\big|_{t^{\mathrm{e}}=0} \begin{pmatrix} \sum_{n,m}\alpha^n_{k,p}\Phi^n_{k-p}\alpha^m_{p',k'}\Phi^m_{p'-k'} & \sum_n \alpha^n_{k,p}\Phi^n_{k-p}t^{\mathrm{e}}_{p,k'} \\ \sum_n t^{\mathrm{e}}_{k,p}\alpha^n_{p',k'}\Phi^n_{p'-k'} & 0 \end{pmatrix} + \mathcal{O}[(t^{\mathrm{e}})^2] \tag{17}$$

in leading order in t^{e}. The diagonal term describes the scattering from low-energy fermions to off-shell states and vice versa via a boson exchange, which could be described via an new effective electron-boson vertex, see Fig. 4(a). In the following, we will neglect this term as it should only give us important corrections for our fermionic quasiparticles for high-energies and not for the low-energy theory since here the dominant processes are the scattering processes between on-shell electrons. In contrast, the off-diagonal terms shown in Fig. 4(b) and (c) give us new relevant physics: The tunneling process from a tip to an off-shell state in the superconductor and from there an inelastic scattering to a state near the Fermi surface via the excitation/absorption of a boson and vice versa.
From (16) it is clear that the Dyson equation for $G^{>,>,ss}_{k,k'}\big|_{t^{\mathrm{e}}=0}$ reads

$$\begin{aligned} G^{>,>,ss}_{k,k'}\big|_{t^{\mathrm{e}}=0} &= \hat{G}^{s,>}_{k,0}\delta_{k,k'} + \int_p G^{s,>}_{k,0}\sum_n \alpha^n_{k,p}\Phi^n_{k-p}G^{>,>,ss}_{p,k'} \\ &\approx \frac{\theta(|\boldsymbol{k}|-k_<)}{-D}\left[\delta_{k,k'} + \int_p \sum_n \alpha^n_{k,p}\Phi^n_{k-p}G^{>,>,ss}_{p,k'}\right] \\ &= \frac{\theta(|\boldsymbol{k}|-k_<)}{-D}\left[\delta_{k,k'} + \sum_n \frac{\alpha^n_{k,k'}\Phi^n_{k-k'}}{-D} + \int_{p^>}\sum_{n,m}\frac{\alpha^n_{k,p}\Phi^n_{k-p}\alpha^m_{p,k'}\Phi^m_{p-k'}}{(-D)^2} + \ldots\right] \end{aligned} \tag{18}$$

In the end we approximated the bare off-shell propagators $\hat{G}^{s,>}_{k,0} \approx -1/D\,\theta(|\boldsymbol{k}|-k_<)$, where D is the band-width of the system, as explained in the main text. Inserting (18) into (17)

we find the following effective low-energy action (14)

$$S_{\text{eff}} = \overbrace{S_{\Phi}^{\text{screen}} + S_{\text{el}}^{<} + S_{el-\Phi}}^{S_0^{\text{screen}}} - \left(\int_{k^<,k'^<} \left[t^{\text{e}}_{k,k'} + \int_{p^>} \sum_n \alpha^n_{k,p} \Phi^n_{k-p} t^{\text{e}}_{p,k'} + \ldots \right] \bar{\psi}_{k,s} \psi_{k',t} + \text{h.c.} \right) \tag{19}$$

The S_0^{screen} described the low energy electrons (and bosons) in the tip and the superconductor in the absence of tunneling. This system can be calculated using the usual field-theoretical models like the Midgal-Eliashberg theory. The low-energy tunneling part of the action has not only an elastic part, but also acquires additional one- and multiple-boson inelastic channels. Rewriting this in terms of an Hamiltonian, we end up with the low-energy tunneling Hamiltonian given in the main text.

DERIVATION OF THE TUNNELING CURRENT FOR THE SPIN-FERMION MODEL

Performing usual perturbation theory to leading order in t^{e}, the elastic contribution[37] of the STM current into a superconductor is just given by the usual Landauer-Büttinger expression (note that we defined the bias here $U = \mu_T - \mu_T$)

$$I^{\text{e}}(U) = 4\pi e \left| t^{\text{e}} \right|^2 \int_{-\infty}^{\infty} d\omega \big[n_F(\omega - eU) - n_F(\omega) \big] \nu_S(\omega) \nu_T(\omega - eU) \tag{20}$$

where we used the approximation $t^{\text{e}}_{\boldsymbol{k},\boldsymbol{k}'} \approx t^{\text{e}}$, and $\nu_{S/T}$ are the fermionic DOS in the superconductor/tip. The inelastic current can be directly computed from the many-body Hamiltonian in the main text using field-theoretical methods[37] and is given by

$$\begin{aligned} I^{\text{i}}(U) = \frac{4\pi e \left| t^{\text{i}} \right|^2}{\nu_S^0} \int_{-\infty}^{\infty} d\omega_1 d\omega_2 \\ \Bigg(& \alpha^2 F_{\text{tun}}(\omega_1)\, \nu_S(\omega_2) \nu_T(\omega_2 - \omega_1 - eU) \\ & \Big[n_F(\omega_2 - \omega_1 - eU) n_B(\omega_1) \big[1 - n_F(\omega_2) \big] - n_F(\omega_2) \big[1 + n_B(\omega_1) \big] [1 - n_F(\omega_2 - \omega_1 - eU) \Big] \\ & + \alpha^2 F_{\text{tun}}(\omega_1)\, \nu_S(\omega_2) \nu_T(\omega_2 + \omega_1 - eU) \\ & \Big[n_F(\omega_2 + \omega_1 - eU) \big[1 + n_B(\omega_1) \big] \big[1 - n_F(\omega_2) \big] - n_F(\omega_2) n_B(\omega_1) [1 - n_F(\omega_2 + \omega_1 - eU)] \Big] \Bigg) \end{aligned}$$

where we defined ν_S^0 as the normal state DOS of the superconductor at the Fermi surface and

$$\alpha^2 F_{\rm tun}(\omega) = \frac{\nu_S^0}{2} \sum_{\substack{\boldsymbol{q},n,m \\ \sigma,\sigma'}} \alpha^n_{\boldsymbol{q},\sigma,\sigma'} \left[\alpha^m_{\boldsymbol{q},\sigma',\sigma}\right]^* \frac{\chi^R_{\boldsymbol{q},nm}(\omega) - \chi^A_{\boldsymbol{q},nm}(\omega)}{-2\pi i} \tag{21}$$

and $\chi^R_{\boldsymbol{q},nm}(t,t') = -i\theta(t-t')\langle \left[\hat{\Phi}^n_{\boldsymbol{q}}(t), \hat{\Phi}^m_{-\boldsymbol{q}}(t')\right] \rangle$ is the retarded boson propagator of the superconducting system (of the effective low-energy theory).

For the spin fermion-model it holds $\alpha^n_{\boldsymbol{q},\sigma,\sigma'} = g_{\boldsymbol{q}} \tau^n_{\sigma,\sigma'}$ and $\chi^R_{\boldsymbol{q},nm}(t,t') = \chi^R_{\boldsymbol{q}}(t,t')\delta_{nm}$ such that we find here the bosonic tunneling spectrum $\alpha^2 F_{\rm tun}(\omega) = g^2\chi(\omega)$ as the integrated spin susceptibility

$$\begin{aligned} g^2\chi(\omega) &= \frac{\nu_S^0}{2} \sum_{\substack{\boldsymbol{q},n,m \\ \sigma,\sigma'}} \left|g^2_{\boldsymbol{q}}\right| \tau^n_{\sigma,\sigma'} \tau^m_{\sigma',\sigma}\, \delta_{n,m} \frac{\chi^R_{\boldsymbol{q}}(\omega) - \chi^A_{\boldsymbol{q}}(\omega)}{-2\pi i} \\ &= 3\nu_S^0 \sum_{\boldsymbol{q}} \left|g^2_{\boldsymbol{q}}\right| \frac{\operatorname{Im} \chi^A_{\boldsymbol{q}}(\omega)}{\pi} \end{aligned} \tag{22}$$

In the limit of a constant tip DOS, we can then easily derive the expressions for the differential conductance given in the main text.

[1] Hoffman, J. *et al.* Imaging quasiparticle interference in $Bi_2Sr_2CaCu_2O_{8+\delta}$. *Science* **297**, 1148–1151 (2002).

[2] Roushan, P. *et al.* Topological surface states protected from backscattering by chiral spin texture. *Nature* **460**, 1106–1109 (2009).

[3] Kreisel, A. *et al.* Interpretation of scanning tunneling quasiparticle interference and impurity states in cuprates. *Phys. Rev. Lett.* **114**, 217002 (2015).

[4] McMillan, W. & Rowell, J. Lead phonon spectrum calculated from superconducting density of states. *Phys. Rev. Lett.* **14**, 108–112 (1965).

[5] McMillan, W. L. Transition Temperature of Strong-Coupled Superconductors. *Phys. Rev.* **167**, 331–344 (1968).

[6] Bardeen, J. Tunnelling from a Many-Particle Point of View. *Phys. Rev. Lett.* **6**, 57–59 (1961).

[7] Cohen, M. H., Falicov, L. M. & Phillips, J. C. Superconductive tunneling. *Phys. Rev. Lett.* **8**, 316–318 (1962).

[8] Eliashberg, G. Temperature Green's function for electrons in a superconductor. *Sov. Phys JETP* **12**, 1000 (1961).

[9] Zasadzinski, J., Coffey, L., Romano, P. & Yusof, Z. Tunneling spectroscopy of $Bi_2Sr_2CaCu_2O_{8+\delta}$: Eliashberg analysis of the spectral dip feature. *Phys. Rev. B* **68**, 180504 (2003).

[10] Niestemski, F. *et al.* A distinct bosonic mode in an electron-doped high-transition-temperature superconductor. *Nature* **450**, 1058–1061 (2007).

[11] Shan, L. *et al.* Evidence of a Spin Resonance Mode in the Iron-Based Superconductor $Ba_{0.6}\mathbf{K}_{0.4}Fe_2As_2$ from Scanning Tunneling Spectroscopy. *Phys. Rev. Lett.* **108**, 227002 (2012).

[12] Song, C.-L. *et al.* Imaging the Electron-Boson Coupling in Superconducting FeSe Films Using a Scanning Tunneling Microscope. *Phys. Rev. Lett.* **112**, 057002 (2014).

[13] Chi, S. *et al.* Scanning tunneling spectroscopy of superconducting LiFeAs single crystals: Evidence for two nodeless energy gaps and coupling to a bosonic mode. *Phys. Rev. Lett.* **109**, 087002 (2012).

[14] Valles, J. M. *et al.* Electron tunneling into single crystals of $YBa_2Cu_3O_{7-\delta}$. *Phys. Rev. B* **44**, 11986–11996 (1991).

[15] Cucolo, A. M., Di Leo, R., Nigro, A., Romano, P. & Bobba, F. Linear normal conductance in copper oxide tunnel junctions. *Phys. Rev. B* **54**, R9686–R9688 (1996).

[16] Misra, S. *et al.* Atomic Scale Imaging and Spectroscopy of a CuO_2 Plane at the Surface of $Bi_2Sr_2CaCu_2O_{8+\delta}$. *Phys. Rev. Lett.* **89**, 087002 (2002).

[17] Nishiyama, M. *et al.* Low Temperature Scanning Tunneling Spectroscopy Studies of High J_c $NdBa_2Cu_3O_{7-\delta}$ Single Crystals. *Journal of superconductivity* **15**, 351–354 (2002).

[18] Maggio-Aprile, I., Renner, C., Erb, A., Walker, E. & Fischer, Ø. Direct Vortex Lattice Imaging and Tunneling Spectroscopy of Flux Lines on $YBa_2Cu_3O_{7-\delta}$. *Phys. Rev. Lett.* **75**, 2754–2757 (1995).

[19] Renner, C., Revaz, B., Kadowaki, K., Maggio-Aprile, I. & Fischer, Ø. Observation of the Low Temperature Pseudogap in the Vortex Cores of $Bi_2Sr_2CaCu_2O_{8+\delta}$. *Phys. Rev. Lett.* **80**, 3606–3609 (1998).

[20] Seidel, P. *et al.* Peculiarities of 'tunneling'characteristics observed in HTS/metal point contact junctions. *Physica C: Superconductivity* **282**, 1481–1482 (1997).

[21] Matsuura, S. *et al.* Reproducible superconducting gap on clean surfaces of BiSrCaCuO prepared by etching with a scanning tunneling microscope tip. *Physica C: Superconductivity* **300**,

26–32 (1998).

[22] Jandke, J. *et al.* Scanning tunneling spectroscopy on $SrFe_2(As_{1-x}P_x)_2$. *Phys. Rev. B* **93**, 104528 (2016).

[23] Fasano, Y. *et al.* Local quasiparticle density of states of superconducting $SmFeAsO_{1-x}F_x$ single crystals: Evidence for spin-mediated pairing. *Phys. Rev. Lett.* **105**, 167005 (2010).

[24] Wang, Z. *et al.* Close relationship between superconductivity and the bosonic mode in $Ba_{0.6}K_{0.4}Fe_2As_2$ and Na $(Fe_{0.975}Co_{0.025})$ As. *Nature Phys.* **9**, 42–48 (2013).

[25] Eschrig, M. & Norman, M. R. Neutron Resonance: Modeling Photoemission and Tunneling Data in the Superconducting State of $Bi_2Sr_2CaCu_2O_{8+\delta}$. *Phys. Rev. Lett.* **85**, 3261–3264 (2000).

[26] Abanov, A. & Chubukov, A. V. SIN and SIS tunneling in cuprates. *Phys. Rev. B* **61**, R9241–R9244 (2000).

[27] Manske, D., Eremin, I. & Bennemann, K. H. Analysis of the resonance peak and magnetic coherence seen in inelastic neutron scattering of cuprate superconductors: A consistent picture with tunneling and conductivity data. *Phys. Rev. B* **63**, 054517 (2001).

[28] Rossat-Mignod & Regnault, L. Neutron Scattering Study of the $YBa_2Cu_3O_{6+x}$ system. *Physica C: Superconductivity and Its Applications (Amsterdam, Netherlands)* **185-189**, 86–92 (1991).

[29] Bourges, P. *et al.* High-energy spin excitations in $YBa_2Cu_3O_{6.5}$. *Phys. Rev. B* **56**, R11439–R11442 (1997). URL `http://link.aps.org/doi/10.1103/PhysRevB.56.R11439`.

[30] Yu, G., Li, Y., Motoyama, E. & Greven, M. A universal relationship between magnetic resonance and superconducting gap in unconventional superconductors. *Nature Phys.* **5**, 873–875 (2009).

[31] Inosov, D. *et al.* Normal-state spin dynamics and temperature-dependent spin-resonance energy in optimally doped $BaFe_{1.85}Co_{0.15}As_2$. *Nature Phys.* **6**, 178–181 (2010).

[32] Dahm, T. *et al.* Strength of the spin-fluctuation-mediated pairing interaction in a high-temperature superconductor. *Nature Phys.* **5**, 217–221 (2009).

[33] Yang, J. *et al.* Exchange boson dynamics in cuprates: optical conductivity of $HgBa_2CuO_{4+\delta}$. *Phys. Rev. Lett.* **102**, 027003 (2009).

[34] Dal Conte, S. *et al.* Disentangling the electronic and phononic glue in a high-Tc superconductor. *Science* **335**, 1600–1603 (2012).

[35] Rowell, J. M., McMillan, W. L. & Feldmann, W. L. Phonon Emission and Self-Energy Effects in Normal-Metal Tunneling. *Phys. Rev.* **180**, 658–668 (1969).

[36] Schackert, M. *et al.* Local measurement of the Eliashberg function of Pb islands: enhancement of electron-phonon coupling by quantum well states. *Phys. Rev. Lett.* **114**, 047002 (2015).

[37] Jandke, J., Hlobil, P., Schackert, M., Wulfhekel, W. & Schmalian, J. Coupling to real and virtual phonons in tunneling spectroscopy of superconductors. *Phys. Rev. B* **93**, 060505 (2016).

[38] Kirtley, J. R. & Scalapino, D. J. Inelastic-tunneling model for the linear conductance background in the high-T_c superconductors. *Phys. Rev. Lett.* **65**, 798–800 (1990).

[39] Kirtley, J. R. Inelastic transport through normal-metal superconductor interfaces. *Phys. Rev. B* **47**, 11379–11383 (1993).

[40] Littlewood, P. B. & Varma, C. M. Anisotropic tunneling and resistivity in high-temperature superconductors. *Phys. Rev. B* **45**, 12636–12639 (1992).

[41] Xiao, M.-w. & Li, Z.-z. Elastic and inelastic tunneling between a high-Tc oxide and normal metal. *Physica C: Superconductivity* **221**, 136–142 (1994).

[42] Bennemann, K.-H. & Ketterson, J. B. *Superconductivity: Volume 1: Conventional and Unconventional Superconductors Volume 2: Novel Superconductors* (Springer Science & Business Media, 2008).

[43] Morel, P. & Anderson, P. W. Calculation of the Superconducting State Parameters with Retarded Electron-Phonon Interaction. *Phys. Rev.* **125**, 1263–1271 (1962).

[44] Berthod, C. & Giamarchi, T. Tunneling conductance and local density of states in tight-binding junctions. *Phys. Rev. B* **84**, 155414 (2011).

[45] Abanov, A., Chubukov, A. V. & Schmalian, J. Fingerprints of spin mediated pairing in cuprates. *Journal of Electron Spectroscopy and Related Phenomena* **117**, 129–151 (2001).

[46] Bourges, P. *et al.* Spin dynamics in the metallic state of the high-T c superconducting system YBa 2 Cu 3 O 6+ x. *Physica B: Condensed Matter* **215**, 30–40 (1995).

[47] Christensen, N. *et al.* Dispersive Excitations in the High-Temperature Superconductor $La_{2-x}Sr_xCuO_4$. *Phys. Rev. Lett.* **93**, 147002 (2004).

[48] Abanov, A. & Chubukov, A. V. A Relation between the Resonance Neutron Peak and ARPES Data in Cuprates. *Phys. Rev. Lett.* **83**, 1652–1655 (1999).

[49] Jenkins, N. *et al.* Imaging the Essential Role of Spin Fluctuations in High-T_c Superconductivity. *Phys. Rev. Lett.* **103**, 227001 (2009).